



UNIVERSITY OF LEEDS

This is a repository copy of *Railway ballast anisotropy testing via true triaxial apparatus*.

White Rose Research Online URL for this paper:

<http://eprints.whiterose.ac.uk/161382/>

Version: Accepted Version

Article:

Yu, Z, Connolly, DP, Woodward, PK et al. (2 more authors) (2020) Railway ballast anisotropy testing via true triaxial apparatus. *Transportation Geotechnics*, 23. 100355. ISSN 2214-3912

<https://doi.org/10.1016/j.trgeo.2020.100355>

© 2020, Elsevier. This manuscript version is made available under the CC-BY-NC-ND 4.0 license <http://creativecommons.org/licenses/by-nc-nd/4.0/>.

Reuse

This article is distributed under the terms of the Creative Commons Attribution-NonCommercial-NoDerivs (CC BY-NC-ND) licence. This licence only allows you to download this work and share it with others as long as you credit the authors, but you can't change the article in any way or use it commercially. More information and the full terms of the licence here: <https://creativecommons.org/licenses/>

Takedown

If you consider content in White Rose Research Online to be in breach of UK law, please notify us by emailing eprints@whiterose.ac.uk including the URL of the record and the reason for the withdrawal request.



eprints@whiterose.ac.uk
<https://eprints.whiterose.ac.uk/>

Railway ballast anisotropy testing via true triaxial apparatus

Ze-Long Yu^{1,2}, D. P. Connolly³, P. K. Woodward³, O. Laghrouche², E. Tutumluer⁴,

¹Newcastle University, School of Civil Engineering & Geosciences, Newcastle Upon Tyne, NE1 7RU, UK
E-mail: Zelong.Yu@newcastle.ac.uk

²Heriot-Watt University, Institute for Infrastructure and Environment, Edinburgh, EH14 4AS, UK
E-mail: O.Laghrouche@hw.ac.uk

³University of Leeds, Institute for High Speed Rail and Systems Integration. Leeds, LS2 9JT, UK
E-mail: d.connolly@leeds.ac.uk; P.K.Woodward@leeds.ac.uk

⁴University of Illinois at Urbana-Champaign, Department of Civil and Environmental Engineering, 205 N. Mathews, Urbana, IL 61801, United States
E-mail: tutumlue@illinois.edu

Abstract

This paper aims to demonstrate the highly anisotropic behaviour of railway ballast via true-triaxial tests. To do so, a novel, large-scale, true-triaxial testing apparatus (GeoTT) is designed and constructed. It consists of six hydraulic actuators, designed to apply a distributed stress to large granular cubic test specimens with dimensions: 500mm × 500mm × 500mm. To show the capability of the new facility, crushed granite railway ballast with $d_{50}=43\text{mm}$ is tested. Three different confining stresses are applied to determine the Poisson's ratio and modulus in three dimensions. Anisotropic behaviour is clearly evident, with horizontal directions showing a lower modulus compared to the vertical direction. It is also found that confining stress has an important effect on both Poisson's ratio and modulus when primary loading is applied in three orthogonal directions. These results are useful for understanding the behaviour of railway ballast and for the calibration of railroad numerical models.

Key words: Granular particle anisotropy; Railway ballast; true triaxial testing (GeoTT), modulus; Poisson's ratio; Railroad

1 Introduction

Granular soils are often referred to as aggregates and are a common construction material for pavements and railways. A large number of studies have been undertaken to quantify the isotropic behaviour of granular particles, including (Roscoe et al., 1963; Lade and Duncan, 1975; Van Eekelen, 1980; Sagaseta, 1987; Alonso et al., 1990; Laloui, 2003; Rotta et al., 2003; Alonso et al., 2012). Testing of granular materials with large maximum particle size requires larger-scale testing apparatus compared to the testing of smaller particles. This is because larger sample volumes are required to ensure the ratio between maximum particle size and sample dimension is low.

Although isotropic loading tests provide insights into material behaviour, many granular materials actually behave in an anisotropic manner (Miura et al. 1984, Tutumluer 1995, Tutumluer and Thompson 1997, Tutumluer and Kwon 2009). Table 1

41 outlines a range of studies performed using traditional triaxial cells to explore
42 anisotropy of response. The anisotropic behaviour of ballast is important for railways
43 because it aids the understanding of ballast degradation and thus maintenance costs.
44 In particular, it is an important material input when numerically modelling ballast.

45 However, investigating anisotropy ideally requires the test sample to be
46 subject to a range of stress paths that are difficult to achieve using standard triaxial
47 testing. Therefore, the two most common approaches to achieve this are: Hollow
48 Cylinder Apparatus (HCA) and true triaxial (TT) testing. HCA methods are useful for
49 simulating the rotation of principal stresses that occur during wheel passage.
50 Alternatively, TT methods account for the effect of intermediate principal stresses,
51 which in reality, may be different from the minor principal stresses when considering
52 full anisotropy.

53 HCA works by subjecting a hollow, cylindrical soil sample to an axial load and
54 torque about the central vertical axis, while applying external and internal radial
55 pressures. The torque results in shear stresses while the axial load combined with the
56 radial pressures results in vertical stress (Cooling and Smith, 1936, Hight et al., 1983,
57 Saada, 1988, Grabe, 2003).

58 The majority of HCA research into granular particle anisotropy to-date has
59 focused on materials with relatively small maximum particle size (see Table 2). For
60 example, Tatsuoka *et al.* (1986), Pradhan et al. (1988a) and Pradhan et al. (1988b)
61 tested soil specimens with inner diameter, outer diameter and height of 60mm,
62 100mm and 200mm, respectively. They investigated the strength and deformation
63 properties of Toyoura sand. Alternatively, Yang et al. (2007) used larger HCA
64 apparatus to investigate the anisotropic behaviour of saturated sand. Alternatively,
65 Lade, Nam and Hong (2008) and Lade (2008) used HCA tests to study the cross-
66 anisotropic behaviour of Santa Monica beach sand and found that cross-anisotropy
67 correlated with increasing inclinations of the major principal stress direction. O'Kelly
68 and Naughton (2005), O'Kelly and Naughton (2009), Yang (2013), Yang et al. (2016)
69 and Rolo (2004) also used HCA testing to investigate the anisotropic behaviour of
70 sands.

71 As an alternative to HCA testing, TT testing works by subjecting a soil sample
72 to stresses in the three orthogonal planes, often using two hydraulic actuators in each
73 plane, either via rigid flat plates or flexible membranes or a mixture of both (see Table
74 3 for a summary of previous studies). Selig et al. (1979) and Desai et al. (1983)
75 developed true triaxial test setups to apply a three-dimensional, independently
76 controlled, and compressive stress state, using fluid or pneumatically pressurized
77 flexible cushions to transmit stresses in three orthogonal directions, to a cubic sand-
78 ballast specimen with dimensions 101.6mm × 101.6mm × 101.6mm. Isotropic loading
79 was applied to specimens to determine anisotropic response behaviour (i.e.,
80 directional dependencies of compacted specimen responses). Alternatively, Yamada
81 and Ishihara (1979) used true triaxial apparatus with a cubic sand specimen of
82 dimensions 100mm × 100mm × 100mm. Results indicated that behaviour was highly

83 anisotropic, inherently due to grain orientation, size and shape. However, as the
84 applied shear stress increased, at failure, the inherent anisotropic effects
85 disappeared.

86 Alternatively, Reis et al. (2011) developed a cubic triaxial cell to test 60mm
87 specimens of saturated and unsaturated soil. Further, Ochiai and Lade (1983) used
88 true triaxial apparatus to study the anisotropic behaviour of Cambria sand and found
89 that the major principal strain was the lowest when the dilation rate was at a
90 maximum. The same apparatus was then used to develop a failure criterion for cross-
91 anisotropic soils (Abelev and Lade 2003, Abelev and Lade 2004).

92 Furthermore, Tutumluer and Seyhan (1999) and Seyhan and Tutumluer (2002)
93 used a triaxial device to test aggregate samples with 150 mm diameter and 150 mm
94 height. The vertical modulus was found to be larger than the horizontal modulus for
95 all tested aggregates except one gravel specimen which contained 16% fines (defined
96 as passing the No. 200 sieve or smaller than 0.075 mm) in a dense-graded base course
97 aggregate with a maximum size of 25 mm.

98 When testing granular particles, it is important to maximise the sample size-
99 to-particle ratio, defined as the minimum dimension of the test sample divided by
100 maximum particle size. If too small, individual particles dominate test results thus
101 causing testing errors. As a guide, Nitchiporovitch (1969) and Fagnoul and
102 Bonnechere (1969) suggested a minimum sample size-to-particle ratio of 5, while
103 Marachi et al. (1972) proposed a ratio of 6. Therefore, because the width of the HCA
104 wall is relatively thin, it is not well-suited for testing large diameter particles. True
105 triaxial apparatus is arguably better suited because it can house a cuboidal volume of
106 granular material, with potentially larger dimensions than the HCA. However, even
107 then, it is challenging to construct a TT apparatus of sufficient scale to investigate
108 anisotropy of samples containing large granular particles.

109 This paper addresses these sample size challenges by developing a new TT facility
110 capable of testing soil samples with dimensions: 500mm x 500mm x 500mm. The
111 large potential test volume means it is well suited to testing large-particle granular
112 soils, including railway ballast. The maximum particle size tested in this study was
113 63mm, giving a sample size-to-particle ratio of approximately 8. The facility was used
114 to apply tri-directional stress patterns to railroad ballast and investigate its
115 anisotropic behaviour. Since the previous research was focused on the study between
116 confining stress and Poisson's ratio in the vertical direction only. This paper extended
117 this concept and revealed the relationship between confining stress and Poisson's
118 ratio in the horizontal direction.

119

120 Table 1. Anisotropic tests conducted using traditional triaxial cells

Source	Soil type	Dimension (mm)	Aim
--------	-----------	----------------	-----

Miura, Seiichi and Toki (1984)	Sand	Diameter =70mm, Height = 170mm	Anisotropy, stress-strain curves, liquefaction
Tutumluer and Seyhan (1999) and Seyhan and Tutumluer (2002)	Aggregate	Diameter =150mm Height =150mm	Anisotropy, resilient behaviour
Rolo (2004)	Sand/clay	Diameter =100mm Height =200mm	Anisotropy, shear strength
Aursudkij, McDowell and Collop, (2009)	Ballast	Diameter =150mm Height =450mm	Resilient modulus and Poisson's ratio
Ngo, Indraratna and Rujikiatkamjorn (2017)	Ballast	Diameter =300mm Height =600mm	Anisotropy behaviour, mobilized friction angle

121

122

Table 2. Anisotropic tests conducted using hollow cylinder apparatus

Source	Soil type	Inner diameter/ Outer diameter/ Height (mm)	Aim
Hight, Gens and Symes (1983),	Sand/clay	203/254/254	Principal stress rotation effects
Tatsuoka <i>et al.</i> (1986),	Sand	30/50/200	Anisotropy, shear strength
Pradhan, Tatsuoka and Horii (1988), Pradhan, T.B.S., Tatsuoka, F. and Horii (1988)	Sand	60/100/200	Anisotropy, shear strength
Grabe (2003)	Sand	60/100/200	Principal stress rotation effects, anisotropy
Rolo (2004)	Sand/clay	76/100/200	Anisotropy shear strength
Yang, Li and Yang (2007)	Sand	150/314/200	Anisotropy, intermediate principal stress
Lade, Nam and Hong (2008) and Lade (2008)	Sand	180/220/400	Principal stress rotation effects, anisotropy, Shear strength
O'Kelly and Naughton (2005) and O'Kelly and Naughton (2009)	Sand	71/100/200	Anisotropy, small strain, yield criterion
Yang (2013), Yang et al. (2016)	Sand	60/100/200	Anisotropy, plasticity, non-coaxiality

123

124

125

Table 3. Anisotropic tests conducted using true triaxial test apparatus

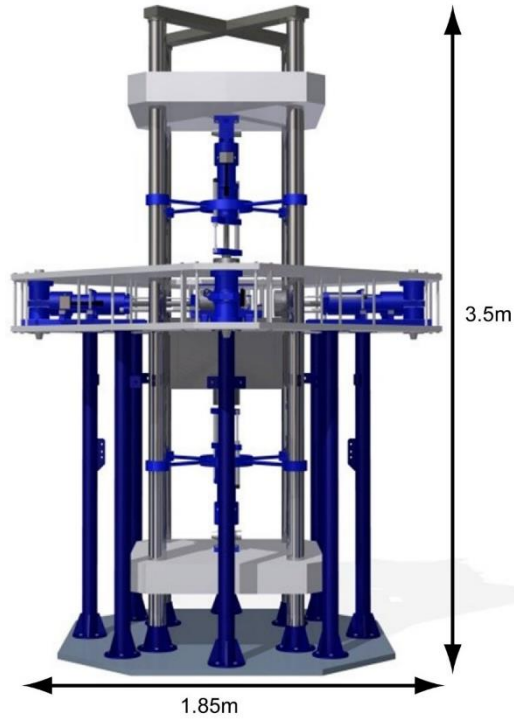
Source	Soil type	Dimension of cubic sample side length (mm)	Aim
Yamada and Ishihara (1979)	Sand	100mm	Anisotropy, shear strength
Selig, Sture and Desai (1979) and Desai, Siriwardane and Janardhanam (1983)	Sand/ballast	101.6mm	Anisotropy, stress-strain curves
Ochiai and Lade (1983)	Sand	76mm	Anisotropy, stress-strain behaviour
Reis et al. (2011)	Sand	60mm	Anisotropy, saturated and unsaturated
GeoTT (present project)	Railway ballast	500mm	Anisotropy, Poisson's ratio, modulus

126

127 2 Apparatus development

128 2.1 True triaxial test rig

129 A true triaxial testing facility (hereafter called 'GeoTT') was designed for large granular
 130 particle testing in collaboration between Heriot Watt University and The University of
 131 Glasgow. It is 3.5m high and 1.85m wide, with the ability to house test samples with
 132 maximum lateral dimensions of 580mm (Figure 1). It consists of 6 independent
 133 hydraulic actuators, with 2 aligned in each Cartesian plane, making it well-suited for
 134 the large-scale testing of anisotropic behaviour (Figure 2). Also, using 6 rams instead
 135 of 3 means that a more uniform stress distribution can be applied to test samples.
 136 Thus, the effect of varying confining stress can be investigated. Each ram is connected
 137 to a load cell and a linear variable displacement transducer (LVDT) for control
 138 purposes. The control setup allows for a wide range of independent signal types to be
 139 fed into each ram.



140

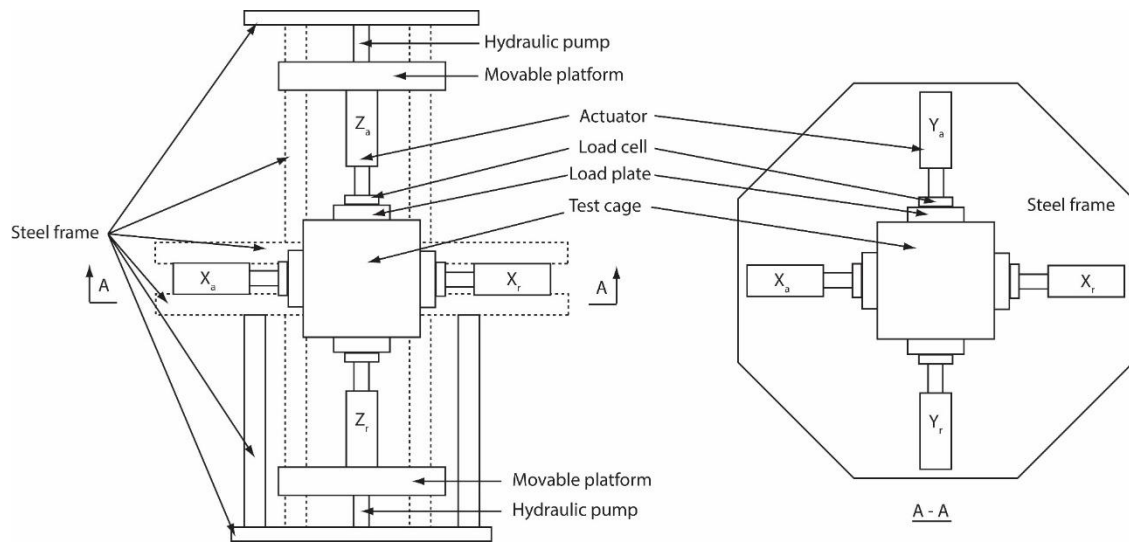
141

142

(a)

(b)

Figure 1. True triaxial testing apparatus: (a) Photograph, (b) Design drawing



143

144

145

Figure 2. Schematic of the GeoTT (Left: side view, Right Birdseye view – not to scale)

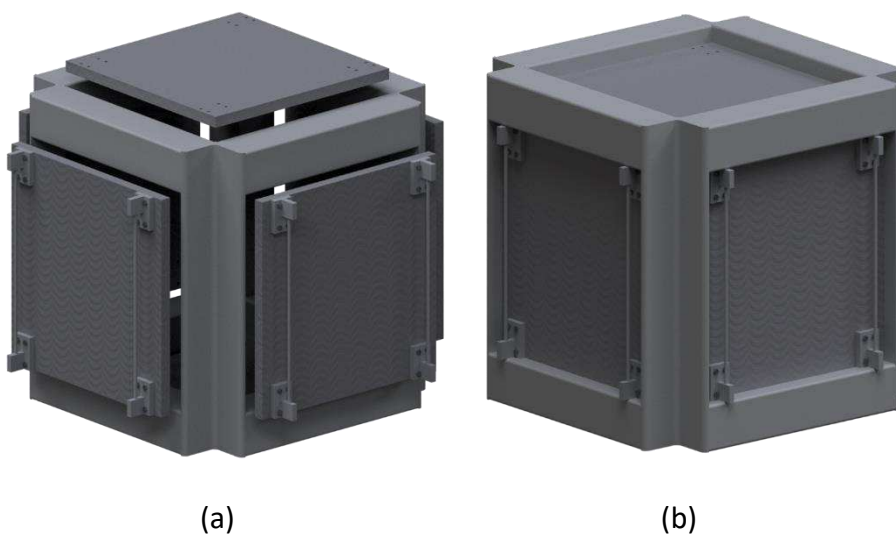
146 2.2 Test cage

147 A bespoke steel test cage was developed to confine the large granular particles during
 148 testing. The outer skeleton had dimensions, 560mm x 560mm x 560mm, and 6
 149 hollow sides. Each of these sides housed 6 separate and independently movable walls
 150 that allowed the sample to change volume during testing (Figure 3). Each wall had a
 151 maximum stroke of 60mm to prevent each wall colliding. The skeleton had

152 protruding protective stops (not shown) to prevent sample egress in the event of
153 excessive wall contraction (Figure 3a). These stops were linked to the control
154 software and the test would automatically halt if this condition was reached. Further,
155 to prevent small granular particles from exiting the sample via the skeleton-wall
156 clearance, the inner test cage was encased using a thin plastic membrane (see Figure
157 4).

158 The true triaxial tests also depended upon the cage wall movement being
159 independent from the cage skeleton. If friction was encountered at this location then
160 the metal-on-metal contact could have introduced testing errors. During initial rig
161 development it was found that this friction risk was greatest in the vertical plane, due
162 to potential sag of the horizontally orientated rams. Therefore a suspension system
163 was developed to support the self-weight of the steel walls and load cells, thus
164 counteracting the downward vertical force on the horizontal rams (Figure 5a). This
165 was implemented by connecting the cage walls to the upper GeoTT frame via
166 tuneable-length steel wires.

167 To illustrate the performance of the suspension system, Figure 5b shows a test
168 performed during GeoTT commissioning, where the position of a lateral cage wall was
169 cycled between the inside and outside of the cage skeleton. At time prior to 800s
170 (shown by the black line), the suspension system was not engaged, however after
171 800s it was engaged. At all data points the measured horizontal force was recorded
172 to quantify the potential horizontal resistance due to friction. In absence of the
173 suspension system, the force varied from -0.20kN to 0.12kN depending upon position,
174 while when present the force varied from -0.09kN to 0.04kN. Therefore, when the
175 suspension system was engaged, the friction between walls and cage skeleton was
176 significantly reduced. Accordingly, the suspension system was used for all tests
177 presented in this paper.



178

179

180

Figure 3. GeoTT testing cage: (a) walls contracted, (b) walls compressed

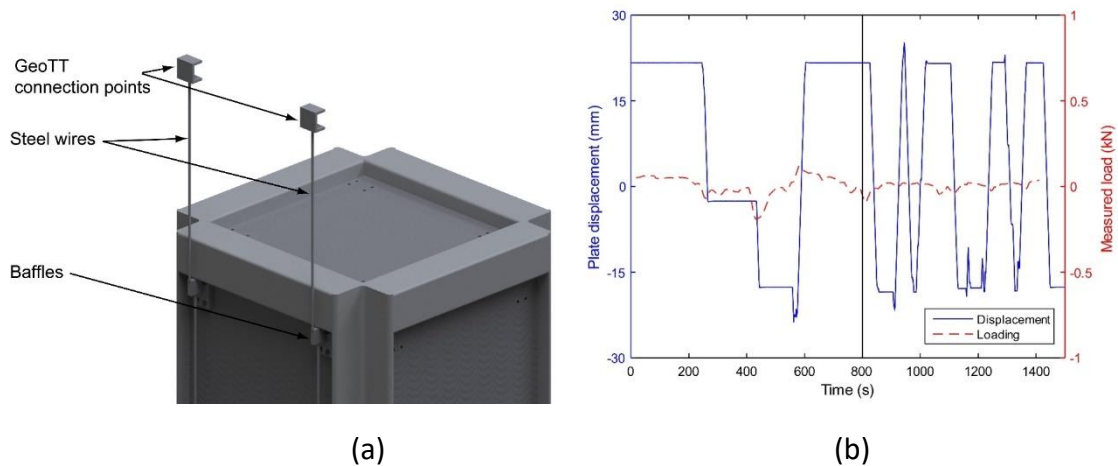


Figure 4. Inner cage with plastic sheet

181

182

183



184

185

Figure 5. Suspension system details: (a) suspension design, (b) wall-skeleton friction

187 3 Testing methodology

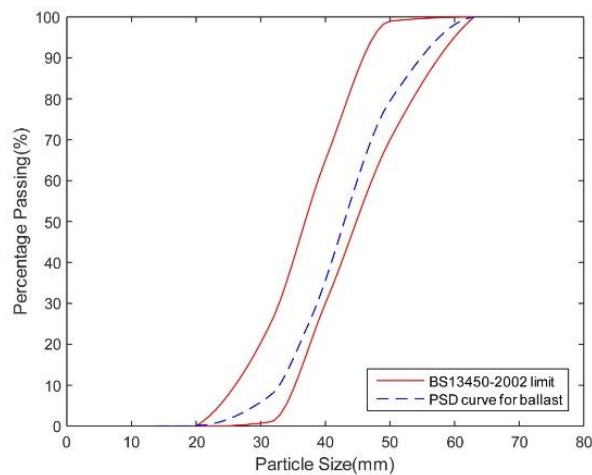
188 Two sets of tests were undertaken. First, monotonic axial loading tests were
 189 performed for the purpose of investigating the Poisson's ratio and modulus of ballast.
 190 Next, a combined hydrostatic loading and unloading test was performed to further
 191 investigate the cross-anisotropic behaviour of ballast. Both tests following
 192 independent loading plans.

193 3.1 Sample preparation

194 The particle size distribution (PSD) of the railway ballast material was characterised in
 195 accordance with BS EN 13450-2002 (BSI, 2002) / BS EN 13450-2013 (BSI, 2013), with
 196 all particles lying in the 20-63mm range and $d_{50} = 43\text{mm}$ (see Figure 6). The coefficient
 197 of uniformity C_u and coefficient of curvature C_c were determined as 1.36 and 1.009
 198 respectively, indicating the ballast was classified as uniformly graded. The ballast

199 aggregate was also washed and dried in accordance with EN 13450-2002 (BSI, 2002) /
 200 BS EN 13450-2013 (BSI, 2013) and BS EN 933-1 (BSI, 2005). After the ballast was
 201 prepared, it was poured into the test cage (500mm x 500mm x 500m) in 5 stages,
 202 and each layer was compacted for exactly 10 minutes using a vibrating Kango tool to
 203 achieve a specimen density of 1,300kg/m³.

204 Although only particle size distribution tests were used to characterise the ballast, it
 205 was sourced from the same Network Rail approved quarry as the ballast used by
 206 Kwan, (2006). Therefore the properties were likely to have been similar to those
 207 found in other UK ballast research works [e.g. LAA index ≤ 20 (BSI, 2010), MDE index
 208 ≤ 7 (BSI, 2011), ACV $\leq 22\%$ (BSI, 1990), Flakiness index ≤ 35 (BSI, 2012), Particle length
 209 ≤ 4 (BSI, 1996)].



210

211 *Figure 6. Ballast particle size distribution curve*

212 **3.2 Test 1: monotonic Axial Loading**

213 The six rams ($X_a, X_r, Y_a, Y_r, Z_a, Z_r$) were used to apply static compressive stresses
 214 towards ballast samples as shown in Figure 7. Subscripts 'r' and 'a' are used to
 215 differentiate between the 2 different rams in each Cartesian plane. The axial load
 216 direction was varied between the X, Y and Z planes, and had a maximum value of
 217 500kPa. Three different confining stresses (30, 60, 75kPa) were applied to the four
 218 specimen faces and each test (e.g. M1-9) was repeated three times, resulting in a
 219 total of 27 test results. The selection of these three confining stresses was based on
 220 the research from Indraratna et al. (2009), where three degradation zones were
 221 identified with confining stress: less than 30kPa, 30-75kPa and larger than 75kPa. For
 222 each test, the following procedure, also summarized in Table 4, was used:

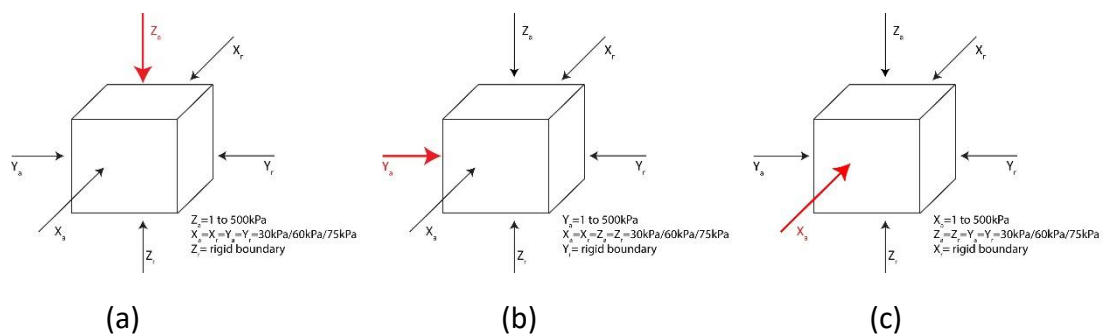
- 223 a) A constant confining stress (either 30kPa/60kPa/75kPa) was applied to the
- 224 ballast sample in the 2 directions that were not the primary loading direction;
- 225 b) The position of the loading plate was recorded to determine the initial length
- 226 of the sample (L);
- 227 c) An axial stress was applied in the primary loading direction and increased

- 228 monotonically at a rate of 62.5kPa per minute, from an initial value of
 229 6.25kPa. The opposite ram maintained a fixed position, thus creating a rigid
 230 boundary;
- 231 d) When the axial stress reached 500kPa, it was held constant for 5 minutes;
 232 e) The axial stress was decreased at a rate of 62.56kPa per 10 seconds until
 233 reaching a magnitude of 6.25kPa;
- 234 f) X, Y and Z displacements were recorded throughout steps a-e;
 235 g) Steps a-f were repeated three times on the sample to ensure repeatability
 236 and consistency of results;
- 237 h) Steps a-g were repeated for the remaining axial loading directions; and finally,
 238 i) The confining stress was increased (3 values tested: 30kPa/60kPa/75kPa) and
 239 steps a-h repeated.
 240

241 *Table 4. Monotonic axial test procedure*

Test stage	Confining stress (kPa)	Confining direction	Axial load direction	Rigid boundary
M1	30	X and Y	Za	Zr
M2	30	X and Z	Ya	Yr
M3	30	Y and Z	Xa	Xr
M4	60	X and Y	Za	Zr
M5	60	X and Z	Ya	Yr
M6	60	Y and Z	Xa	Xr
M7	75	X and Y	Za	Zr
M8	75	X and Z	Ya	Yr
M9	75	Y and Z	Xa	Xr

242



245 Figure 7. Axial load directions: (a) Z_a loading, (b) Y_a loading, (c) X_a loading

246

247 3.3 Test 2: combined Hydrostatic Loading and Unloading

248 In addition to the monotonic axial loading tests, a combined hydrostatic loading and
 249 unloading test was also performed to investigate the unloading response of ballast.
 250 Rather than using the same procedure as for the previous monotonic tests (Table 4),
 251 the hydrostatic compression test procedure outlined by Desai, Siriwardane and
 252 Janardhanam (1983) was used and is summarized in Table 5:

- 253 a) A hydrostatic confining stress of 34.5kPa was applied in all 3 directions
 254 b) The axial stress was increased in increments of 34.5kPa, from the confining
 255 stress (34.5kPa) to 172kPa. At each increment, the deformations were
 256 measured after they stabilized.
 257 c) The axial stress was reduced from 172kPa to 34.5kPa in 34.5kPa increments
 258 d) The axial stress was increased in increments of 34.5kPa, from the confining
 259 stress (34.5kPa) to 345kPa. At each increment, the deformations were
 260 measured after they stabilized.
 261 e) The axial stress was reduced from 345kPa to 34.5kPa, in 34.5kPa increments
 262 f) The axial stress was increased in increments of 34.5kPa, from the confining
 263 stress (34.5kPa) to 517kPa. At each increment, the deformations were
 264 measured after they stabilized.
 265 g) The axial stress was reduced from 517kPa to 34.5kPa, in 34.5kPa increments;
 266 h) The test was repeated for the remaining two Cartesian planes.
 267

268 *Table 5. Hydrostatic testing procedure*

Test stage	Confining stress (kPa)	Deviator stress (kPa)	Confining direction	Axial load direction	Rigid boundary
H1	34.5	137.5	X and Y	Z _a	Z _r
H2	34.5	310.5	X and Z	Y _a	Y _r
H3	34.5	482.5	Y and Z	X _a	X _r

269

270 3.4 Interpretation of test results

271 When a uniaxial compressive force is applied to a cubic or cuboidal test specimen, it
 272 contracts in the axial direction and expands in the remaining two
 273 perpendicular/transverse directions (Figure 8). Assuming the axial stress is in the Z
 274 direction, the resulting recoverable horizontal strains are in the X and Y directions
 275 (see Figure 9). For this case, Equations (1), (2) and (3) give the calculation for the axial
 276 recoverable strain in the Z direction and the horizontal (or transverse) recoverable
 277 strains in X and Y directions, respectively. Then, the magnitude of average horizontal
 278 or transverse strain is calculated using Equations (4):

$$279 \quad \varepsilon_{axial} = \frac{\delta_z}{L}, \text{ (positive for axial compression)} \quad (1)$$

$$280 \quad \varepsilon_{trans_x} = \frac{\delta_x}{L}, \text{ (negative for axial compression)} \quad (2)$$

$$281 \quad \varepsilon_{trans_y} = \frac{\delta_y}{L}, \text{ (negative for axial compression)} \quad (3)$$

$$282 \quad \varepsilon_{trans} = \frac{\varepsilon_{trans_x} + \varepsilon_{trans_y}}{2} \quad (4)$$

283 Where,

284 L is the initial length of the ballast sample

285 δ_x is the recoverable displacement of ballast sample in X direction

286 δ_y is the recoverable displacement of ballast sample in Y direction

287 δ_z is the recoverable displacement of ballast sample in Z direction

288

289 Thus, Poisson's ratio is calculated as:

290
$$\nu = -\frac{\epsilon_{trans}}{\epsilon_{axial}} \quad (5)$$

291 and the modulus is calculated as:

292
$$Modulus = \frac{\sigma_{axial_time}}{\epsilon_{axial_time}} \quad (6)$$

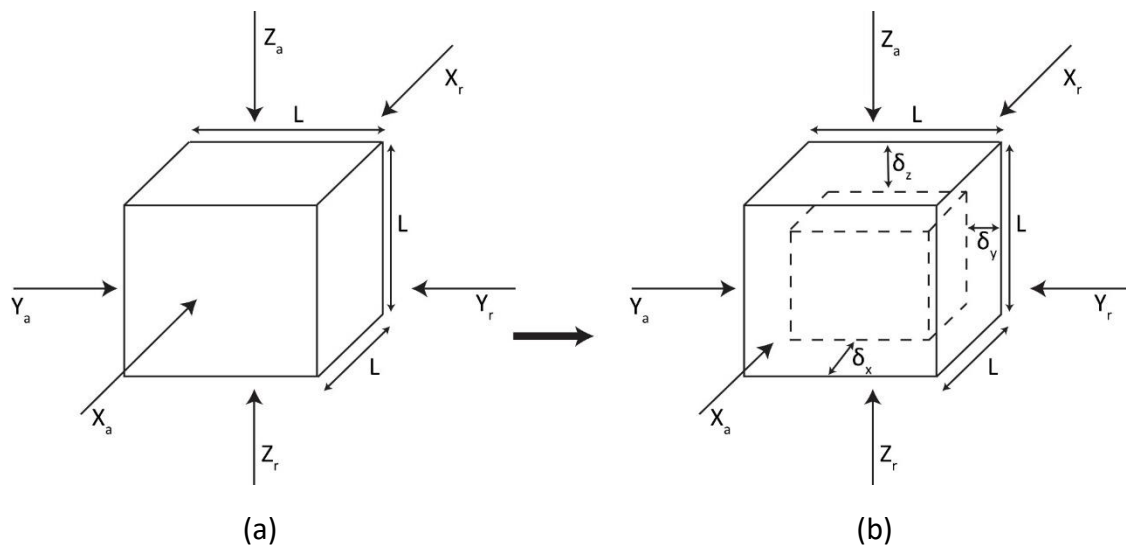
293 Where,

294 σ_{axial_time} is the axial stress time history

295 ϵ_{axial_time} is the axial strain time history

296

297



300 Figure 8. Poisson's Ratio calculation: (a) un-deformed specimen, (b) deformed
301 specimen in dashed line

302

303 4 Test results and discussion

304 4.1 Test 1 results

305 4.1.1 Poisson's ratio

306 For each confining stress and axial load pair, 3 tests were performed. As an example,
307 Figure 9 shows the loading path and displacements in X, Y and Z directions for
308 monotonic axial loading in the Z_a direction under a confining stress of 75kPa. The
309 displacements were used for the calculation of strains, while only recoverable strains
310 were used for the calculation of Poisson's ratio. It is seen that deformation did not
311 return to zero after unloading, thus indicating plastic deformation or displacement.
312 This plastic deformation evinced that the further sample compaction was occurred in
313 the vertical direction while the sample expanded in horizontal direction when the
314 primary loading was applied in Z_a .

315 Since 3 repeated tests were performed under the same confining stress and axial load
316 direction, the mean value of Poisson's ratio was calculated to minimize the test error
317 (e.g. the 3 Poisson' ratios in the Z_a direction from stage M1 with 30kPa confining
318 were averaged, giving a mean Poisson's ratio of 0.31).

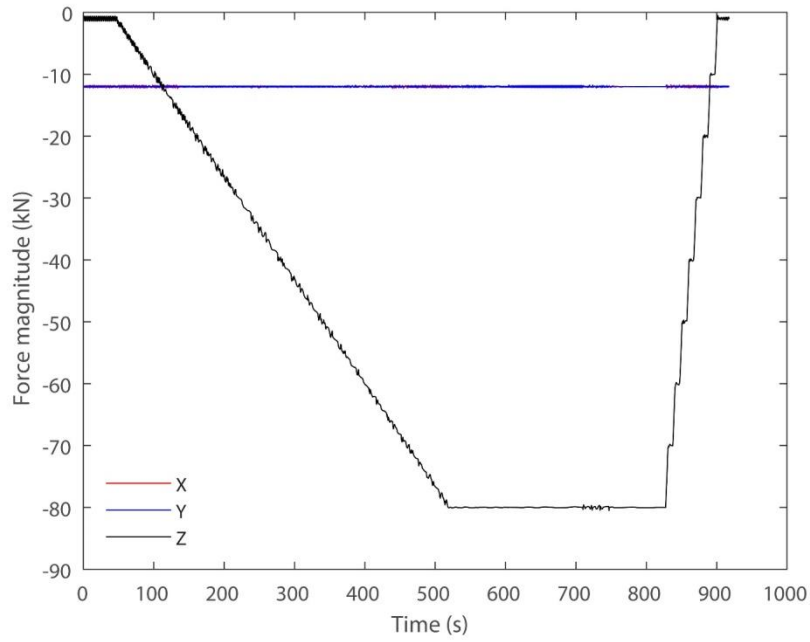
319 Figure 10 shows the relationship between confining stress and Poisson's ratio. It is
320 seen that there was a distinct correlation, with Poisson's ratio decreasing with
321 increased confining stress. The mean values in X, Y and Z directions were 0.28, 0.32
322 and 0.31 at a confining stress of 30kPa. The Poisson's ratio values reduced to 0.22,
323 0.26 and 0.23 for a confining stress of 60kPa and further reduced to 0.15, 0.19 and
324 0.18 for a confining stress of 75kPa (Table 6). This is mainly due to that the increased
325 confining stress reduced the displacement in the confining direction, resulting a
326 reduced Poisson' ratio. This was consistent with the ballast triaxial tests performed by
327 Indraratna et al. (1998), where the initial loading stage was used for the study
328 between confining stress and Poisson's ratio in the vertical direction. It was found
329 that Poisson's ratio decreased with increasing confining stress. Similarly, Aursudkij et
330 al. (2009) carried out cyclic triaxial tests and found that the vertical Poisson's ratio
331 decreased as confining stress increased from 30kPa to 60kPa under axial loading. The
332 small discrepancies between the X and Y directions were likely because the
333 monotonic test in the X direction was performed after the Y direction, resulting a
334 lower Poisson' ratio in the X direction.

335

336 Table 6. Poisson's ratios for monotonic lading in X, Y and Z directions

Confining stress (kPa)	30			60			75		
	X	Y	Z	X	Y	Z	X	Y	Z
Mean value of Poisson's ratio	0.28	0.32	0.31	0.22	0.26	0.23	0.15	0.19	0.18

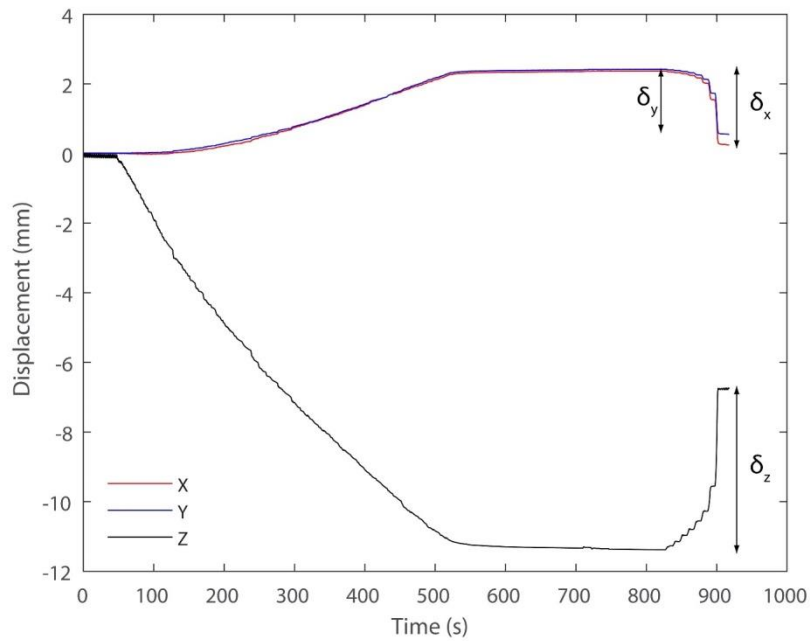
337



338

339

(a)



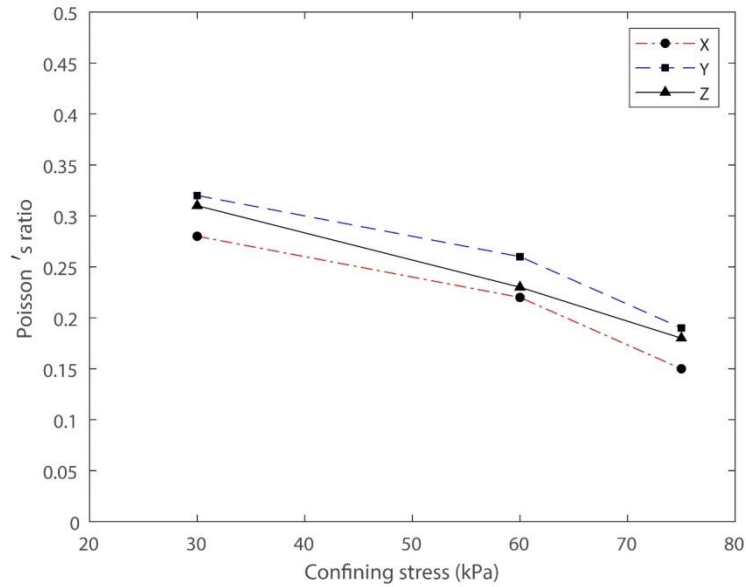
340

341

(b)

342 *Figure 9. Monotonic testing results when loading in Z_0 direction under a confining*
 343 *stress of 75kPa: (a) loading path, (b) displacements in X, Y and Z directions*

344



345

346

Figure 10. Relationship between Poisson's ratio and axial loading direction

347

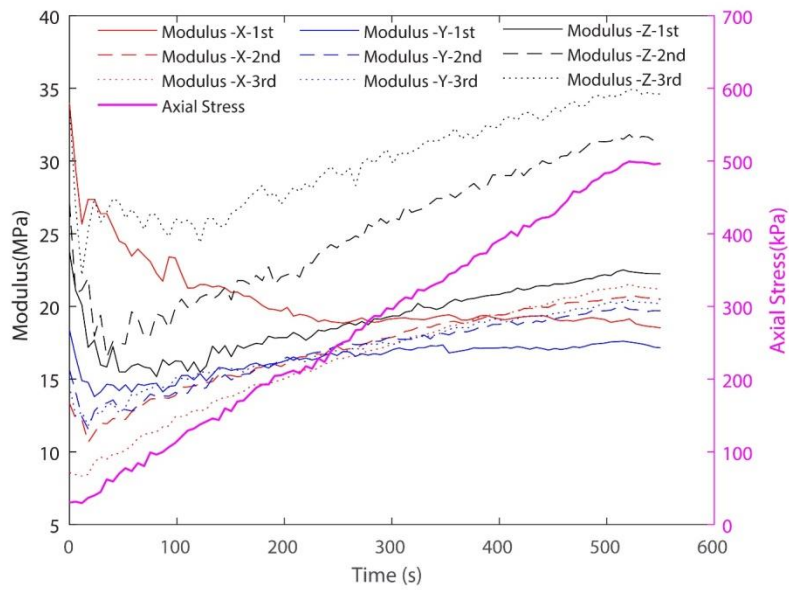
348

349 4.1.2 Modulus

350 Figure 11 shows an example of the modulus from all repeated tests in X, Y and Z axial
 351 load directions under 75kPa confining stress. Correspondingly, Figure 12-Figure 14
 352 show the mean modulus (average modulus across the 3 repeated tests) for confining
 353 stresses of 30, 60 and 75kPa respectively. Considering the Z direction at 30kPa, Figure
 354 12 shows that the modulus decreased rapidly when the axial stress was low, reached
 355 a local minimum and then increased again steadily as axial stress was increased. This
 356 dilation resulted in the modulus at the end of the test (500kPa) being similar to the
 357 starting value. Regarding the X and Y directions, their responses were similar and had
 358 modulus significantly lower than the vertical direction (Z is on average 73% higher
 359 than X, and 66% higher than Y, when the axial stress is 500kPa).

360 Similar findings were obtained for confining stresses of 60kPa and 75kPa. Figure 13
 361 shows the 60kPa case where Z was on average 66% higher than X and 76% higher
 362 than Y when the axial stress was 500kPa. Alternatively, Figure 14 shows the 75kPa
 363 case where Z was on average 46% higher than X and 54% higher than Y when the axial
 364 stress was 500kPa. The overall combined results are shown in Figure 15 where it can

365 be seen that for all directions, the lower confining stress resulted in lower modulus.

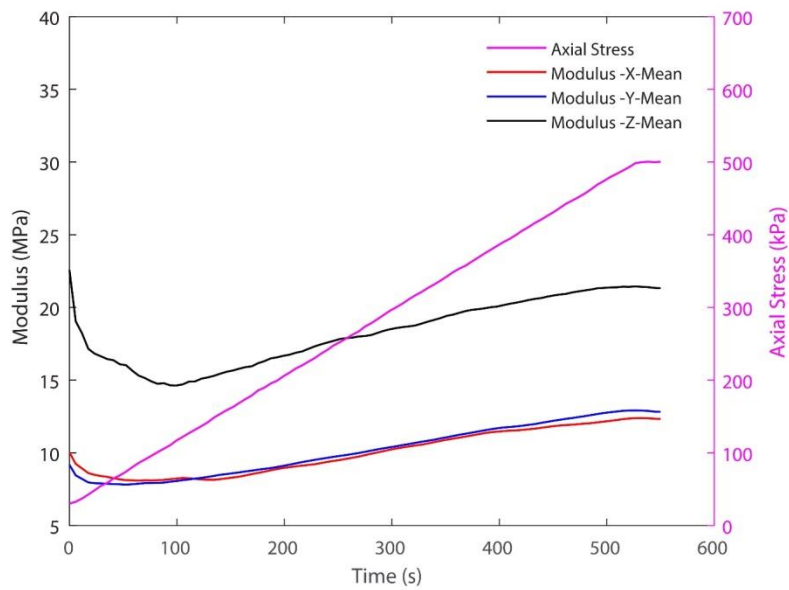


366

367 *Figure 11. Raw modulus in X, Y and Z axial load directions under 75kPa confining stress*

368

369

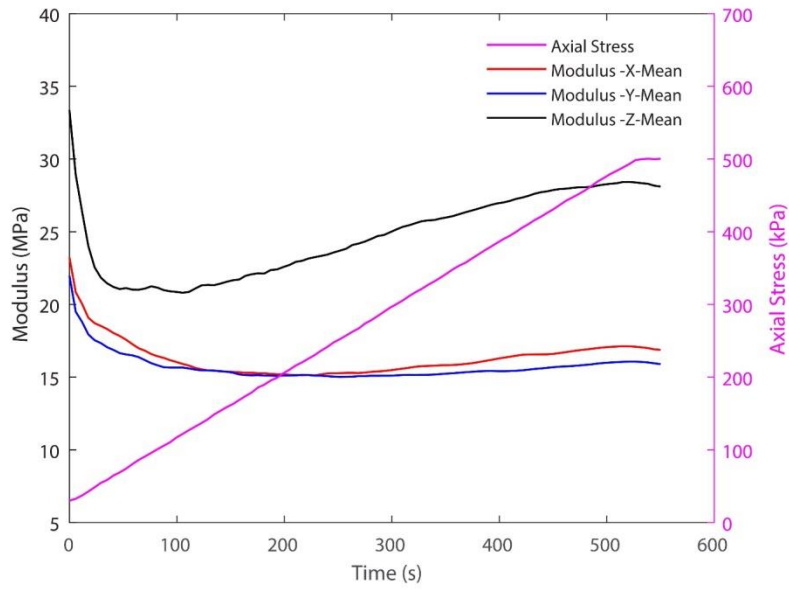


370

371 *Figure 12. Mean modulus in X, Y and Z axial load directions under 30kPa confining*
372 *stress*

373

374



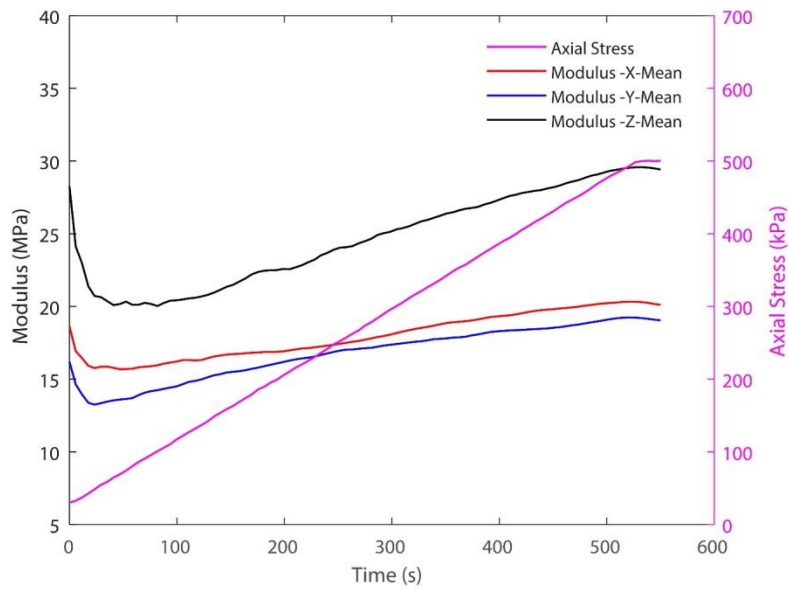
375

376

377

Figure 13. Mean modulus in X, Y and Z axial load directions under 60kPa confining stress

378



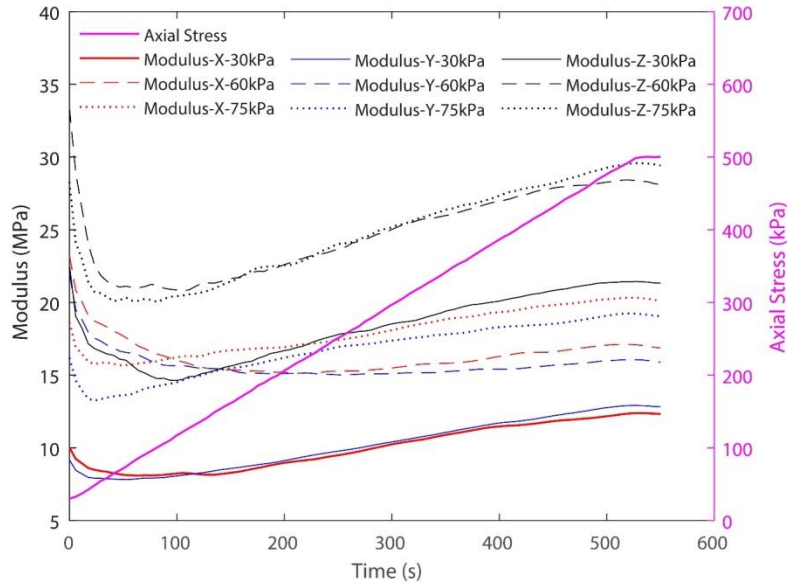
379

380

381

Figure 14. Mean modulus in X, Y and Z axial load directions under 75kPa confining stress

382



383

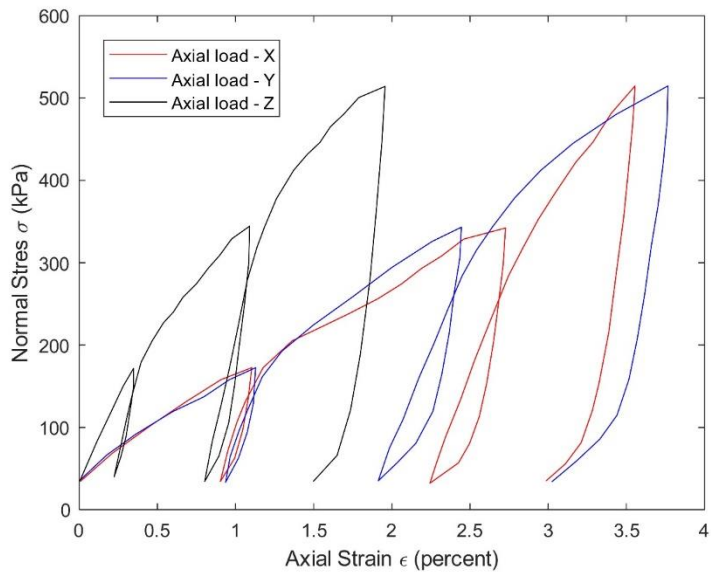
384 *Figure 15. Mean modulus in X, Y and Z axial load directions under varying confining*
 385 *stress*

386

387 4.2 Test 2 results

388 Figure 16 shows the three loading and unloading cycles of the test sample.
 389 Permanent deformation was clearly recorded after the 3 cycles in X, Y, and Z
 390 directions, and reached maximums of 172kPa, 345kPa and 517kPa, respectively. The
 391 horizontal directions (X and Y) exhibited approximately double the permanent
 392 deformation (3%) compared to the vertical direction (1.5%), thus demonstrating the
 393 typical cross-anisotropic behavior of ballast. Based on recoverable strains after each
 394 unloading stage, the relationship between sample modulus and deviator stress is
 395 presented in Figure 17. It shows that sample modulus in the X and Y directions
 396 increased from 640 MPa and 600 MPa, to 800 MPa and 700MPa respectively, when
 397 the deviator stress was 310.5 kPa. However, the sample modulus in the Z direction
 398 increased from 900 MPa to 1000 MPa when deviator stress reached 310.5 kPa, and
 399 then remained constant. This change of modulus in each direction again indicated the
 400 cross-anisotropic behaviour of the ballast sample, while this cross-anisotropic
 401 behaviour was similar in X and Y direction in terms of unloading response and sample
 402 modulus. However, it should be noted that the responses show discrepancies with
 403 traditional nonlinear soil behaviour.

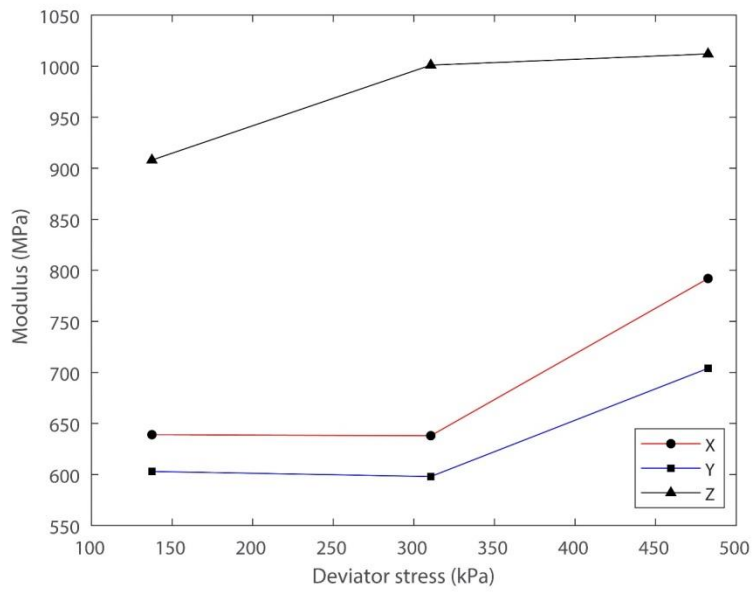
404 Upon inspection after testing, ballast breakage was noticed when removing the
 405 sample from the test cage. Also, ballast aggregate particle cracking was heard during
 406 testing.



407

408

Figure 16. Unloading response in all three axial load directions



409

410

Figure 17. Relationship between modulus and deviator stress

411 5 Conclusions

412 Railway ballast typically behaves in an anisotropic manner, with greater stiffness in
413 the vertical compaction direction. This is important to quantify for a better
414 understanding of the field mechanical behaviour, and for the modelling of the
415 dynamic response behaviour. Therefore, this paper presented results for a railway
416 ballast aggregate material tested under true-triaxial conditions. A novel, large, true-
417 triaxial apparatus and its accompanying testing cage were successfully developed in
418 the laboratory. The true triaxial device utilised six hydraulic actuators to ensure a
419 uniform stress distribution across the test sample. Three confining stresses (30kPa,
420 60kPa and 75kPa) were used to investigate Poisson's ratio, modulus and loading-
421 unloading characteristics. Anisotropic behaviour was clearly observed for the ballast
422 aggregate material; the horizontal response as obtained from horizontal and
423 transverse strain measurements varied when compared to the strain values measured
424 in the vertical direction. Both Poisson's ratio and modulus were sensitive to the
425 applied confining stresses.

426

427 6 Acknowledgement

428 The authors express their gratitude to The University of Glasgow and Prof David Muir
429 Wood for their significant efforts on the original development of the true triaxial rig.
430 They also thank Heriot-Watt University for the support to modify the original design
431 and adaption for ballast testing. Also, support from the University of Leeds is
432 acknowledged along with the financial assistance from the Leverhulme Trust (PLP-
433 2016-270).

434

435

436 7 References

- 437 Abelev, A. V. and Lade, P. V. (2004) 'Characterization of Failure in Cross-Anisotropic Soils',
438 *Journal of Engineering Mechanics*, 130(5), pp. 599–606.
- 439 Abelev, A. V. and Lade, P. V. (2003) 'Effects of cross anisotropy on three-dimensional behavior
440 of sand. I: Stress-strain behavior and shear banding', *Journal of Engineering Mechanics*, 29(2),
441 pp. 160–166.
- 442 Alonso, E. ., Gens, A. and Josa, A. (1990) 'A constitutive model for partially saturated soils',
443 *Géotechnique*, 40(3), pp. 405–430.
- 444 Alonso, E. E., Pinyol, N. M. and Gens, A. (2012) 'Compacted soil behaviour: initial state,
445 structure and constitutive modelling', *Géotechnique*, V1(16), p. 134p.
- 446 Aursudkij, B., McDowell, G. R. and Collop, A. C. (2009) 'Cyclic loading of railway ballast under
447 triaxial conditions and in a railway test facility', *Granular Matter*, 11(6), pp. 391–401.
- 448 BSI (1990) 'BS 812-111. Testing aggregates. Methods for determination of ten per cent fines
449 value (TFV)', *British Standards Institution*.
- 450 BSI (1996) 'BS EN 933-2. Tests for geometrical properties of aggregates. Determination of
451 particle size distribution. Test sieves, nominal size of apertures', *British Standards Institution*.
- 452 BSI (2002) 'BS EN 13450 Aggregates for railway ballast', *British Standards Institution*.
- 453 BSI (2005) 'BS EN 933-1. Tests for geometrical properties of aggregates Part 1: Determination
454 of Particle Size Distribution - Sieving Method', *British Standards Institution*, 3(1), pp. 1–7.
- 455 BSI (2010) 'BS EN 1097-2. Tests for mechanical and physical properties of aggregates.
456 Methods for the determination of resistance to fragmentation', *British Standards Institution*.
- 457 BSI (2011) 'BS EN 1097-1. Tests for mechanical and physical properties of aggregates.
458 Determination of the resistance to wear (micro-Deval)', *British Standards Institution*.
- 459 BSI (2012) 'BS EN 933-3. Tests for geometrical properties of aggregates. Determination of
460 particle shape. Flakiness index', *British Standards Institution*.
- 461 BSI (2013) 'BS EN 13450 Aggregates for railway ballast', *British Standards Institution*.
- 462 Cooling, L. F. and Smith, D. B. (1936) 'The Shearing Resistance of Soils', *Journal of the
463 Institution of Civil Engineering*, 3(7), pp. 333–343.
- 464 Desai, C. S., Siriwardane, H. J. and Janardhanam, R. (1983) 'Interaction and load transfer
465 through track support systems, Parts 2', *Final Rep., DOT/RSPA/DMA-50/83/12, Office of
466 University Research, Dept. of Transportation, Washington, DC*.
- 467 Van Eekelen, H. A. M. (1980) 'Isotropic yield surfaces in three dimensions for use in soil
468 mechanics', *International Journal for Numerical and Analytical Methods in Geomechanics*,
469 4(1), pp. 89–101.
- 470 Fagnoul, A. and Bonnechere, F. (1969) 'Shear strength of porphyry materials', in *Proceedings
471 of the 7th International Conference on Soil Mechanics and Foundation Engineering, Mexico*,
472 pp. 61–65.
- 473 Grabe, P. J. (2003) *Resilient and permanent deformation of railway foundations under
474 principal stress rotation*. PhD Thesis, University of Southampton.
- 475 Hight, D. W., Gens, A. and Symes, M. J. (1983) 'The development of a new hollow cylinder

- 476 apparatus for investigating the effects of principal stress rotation in soils', *Géotechnique*,
477 33(4), pp. 355–383.
- 478 Indraratna, B., Ionescu, D. and Christie, H. D. (1998) 'Shear behavior of railway ballast based
479 on large-scale triaxial tests', *Journal of geotechnical and geoenvironmental Engineering*,
480 124(5), pp. 439–449.
- 481 Indraratna, B., Nimbalkar, S. and Christie, D. (2009) 'The Performance of Rail Track
482 Incorporating the Effects Of Ballast Breakage, Confining Pressure and Geosynthetic
483 Reinforcement', in *Bearing Capacity of Roads, Railways and Airfields. 8th International
484 Conference (BCR2A'09)*.
- 485 Kwan, C. (2006) *Geogrid Reinforcement of Railway Ballast*. PhD Thesis, University of
486 Nottingham.
- 487 Lade, P. V. (2008) 'Failure Criterion for Cross-Anisotropic Soils', *Journal of Geotechnical and
488 Geoenvironmental Engineering*, 134(1), pp. 117–124.
- 489 Lade, P. V. and Duncan, J. M. (1975) 'Elastoplastic stress-strain theory for cohesionless soil',
490 *ASCE J Geotech Eng Div*, 101(10), pp. 1037–1053.
- 491 Lade, P. V., Nam, J. and Hong, W. P. (2008) 'Shear banding and cross-anisotropic behavior
492 observed in laboratory sand tests with stress rotation', *Canadian Geotechnical Journal*, 45(1),
493 pp. 74–84.
- 494 Laloui, L. and Cekerevac, C. (2003) 'Thermo-Plasticity of Clays: An Isotropic Yield Mechanism',
495 *Computers and Geotechnics*, 30(8), pp. 649–660.
- 496 Marachi, N. D., Chan, C. K. and Seed, H. B. (1972) 'Evaluation of properties of rockfill
497 materials', *Journal of Soil Mechanics & Foundations Div*, 97(SM1).
- 498 Miura, Seiichi and Toki, S. (1984) 'Anisotropy in mechanical properties and its simulation of
499 sands sampled from natural deposits', *Soils and Foundations*, 24(3), pp. 69–84.
- 500 Ngo, N. T., Indraratna, B. and Rujikiatkamjorn, C. (2017) 'Micromechanics-Based Investigation
501 of Fouled Ballast Using Large-Scale Triaxial Tests and Discrete Element Modeling', *Journal of
502 Geotechnical and Geoenvironmental Engineering*, 143(2), p. 04016089.
- 503 Nitchiporovitch, A. A. (1969) 'Shearing strength of coarse shell materials', in *Proceedings of
504 the 7th International Conference on Soil Mechanics and Foundation Engineering, Mexico*, pp.
505 211–216.
- 506 O'Kelly, B. C. and Naughton, P. J. (2005) 'Development of a new hollow cylinder apparatus for
507 stress path measurements over a wide strain range', *Geotechnical Testing Journal*. ASTM
508 International, 28(4), pp. 345–354.
- 509 O'Kelly, B. C. and Naughton, P. J. (2009) 'Study of the yielding of sand under generalized stress
510 conditions using a versatile hollow cylinder torsional apparatus', *Mechanics of Materials*.
511 Elsevier, 41(3), pp. 187–198.
- 512 Ochiai, H. and Lade, P. V. (1983) 'Three-Dimensional Behavior of Sand with Anisotropic Fabric',
513 *Journal of Geotechnical Engineering*, 109(10), pp. 1313–1328.
- 514 Pradhan, T.B.S., Tatsuoka, F. and Horii, N. (1988a) 'Simple shear testing on sand in a torsional
515 shear apparatus', *Soils and Foundations, Japanese Society of Soil Mechanics and Foundation
516 Engineering*. The Japanese Geotechnical Society, 28(2), pp. 95–112.
- 517 Pradhan, T.B.S., Tatsuoka, F. and Horii, N. (1988b) 'Strength and deformation characteristics

518 of sand in torsional simple shear', *Soils and Foundations*. The Japanese Geotechnical Society,
519 28(3), pp. 131–148.

520 Reis, R. M. *et al.* (2011) 'Performance of a cubical triaxial apparatus for testing saturated and
521 unsaturated soils', *Geotechnical Testing Journal*, 34(3), p. 1.

522 Rolo, R. (2004) *The anisotropic stress-strain-strength behaviour of brittle sediments*. PhD
523 Thesis, Imperial College London (University of London).

524 Roscoe, K. H., Schofield, A. N. and Thurairajah, A. (1963) 'Yielding of clays in states wetter
525 than critical', *Géotechnique*, 13(3), pp. 211–240.

526 Rotta, G. V. *et al.* (2003) 'Isotropic yielding in an artificially cemented soil cured under stress',
527 *Géotechnique*, 53(5), pp. 493–501.

528 Saada, A. (1988) 'State-of-the-Art Paper: Hollow Cylinder Torsional Devices: Their Advantages
529 and Limitations', in *Advanced Triaxial Testing of Soil and Rock*. 100 Barr Harbor Drive, PO Box
530 C700, West Conshohocken, PA 19428-2959: ASTM International, pp. 766-766–24.

531 Sagaseta, C. (1987) 'Analysis of undraind soil deformation due to ground loss', *Géotechnique*,
532 37(3), pp. 301–320.

533 Seyhan, U. and Tutumluer, E. (2002) 'Anisotropic Modular Ratios as Unbound Aggregate
534 Performance Indicators', *Journal of Materials in Civil Engineering*, 14(5), pp. 409–416.

535 Sture, S. and Desai, C. S. (1979) 'Fluid cushion truly triaxial or multiaxial testing device',
536 *Geotechnical Testing Journal*. ASTM International, pp. 20–33.

537 Tatsuoka, F. *et al.* (1986) 'Failure and deformation of sand in torsional shear.', *Soils and
538 Foundations*. The Japanese Geotechnical Society, 26(4), pp. 79–97.

539 Tutumluer, E. (1995) *Predicting behavior of flexible pavements with granular bases*. PhD
540 Thesis, Georgia Institute of Technology.

541 Tutumluer, E. and Kwon, J. (2009) 'Validations of Anisotropic Aggregate Base Behavior from
542 Full-Scale Pavement Tests', in *Contemporary Topics in Ground Modification, Problem Soils,
543 and Geo-Support*. Reston, VA: American Society of Civil Engineers, pp. 441–448.

544 Tutumluer, E. and Seyhan, U. (1999) 'Laboratory Determination of Anisotropic Aggregate
545 Resilient Moduli Using an Innovative Test Device', *Transportation Research Record: Journal of
546 the Transportation Research Board*, 1687, pp. 13–21.

547 Tutumluer, E. and Thompson, M. R. (1997) 'Anisotropic modeling of granular bases in flexible
548 pavements', *Journal of Transportation Research Board*, TRR 1577(970539), pp. 18–26.

549 Yamada, Y. and Ishihara, K. (1979) 'Anisotropic deformation characteristics of sand under
550 three dimensional stress conditions', *Japanese Society of Soil Mechanics and Foundation
551 Engineering*, 19(2), pp. 79–94.

552 Yang, L. (2013) *Experimental study of soil anisotropy using hollow cylinder testing*. PhD Thesis,
553 University of Nottingham.

554 Yang, L. T. *et al.* (2016) 'A laboratory study of anisotropic geomaterials incorporating recent
555 micromechanical understanding', *Acta Geotechnica*, 11(5), pp. 1111–1129.

556 Yang, Z. X., Li, X. S. and Yang, J. (2007) 'Undrained anisotropy and rotational shear in granular
557 soil', *Géotechnique*. Thomas Telford Ltd, 57(4), pp. 371–384.

558